Dielectrophoretically structured piezoelectric composites with high aspect ratio piezoelectric particles inclusions

D. A. van den Ende,[1,2,3,a)] S. E. van Kempen,[2] X. Wu,[2] W. A. Groen,[1,2] C. A. Randall,[4] and S. van der Zwaag[2]
[1]*Holst Centre/TNO, HTC31, 5605 KN Eindhoven, The Netherlands*
[2]*Novel Aerospace Materials Group, Faculty of Aerospace Engineering, Delft University of Technology, Kluyverweg 1, 2629 HS Delft, The Netherlands*
[3]*TNO (Netherlands Organisation for Applied Scientific Research), Materials Technology, Rondom 1, 5612 AP Eindhoven, The Netherlands*
[4]*Materials Research Institute, The Pennsylvania State University, University Park, Pennsylvania 16801, USA*

(Received 6 February 2012; accepted 19 May 2012; published online 21 June 2012)

Piezoelectric composites were prepared by dielectrophoretic alignment of high aspect ratio piezoelectric particles in a thermosetting polymer matrix. A high level of alignment was achieved in the cured composite from a resin containing randomly oriented high aspect ratio particles. Upon application of an electric field during curing of the resin, the particles were found to rotate with their long axes in the direction of the electric field, before coalescing to form chains. The dielectric and piezoelectric properties of the structured composites are well described by an analytical model for composites containing particles arranged into chains. The influence of degree of rotation and aspect ratio of the individual particles as well as their spacing is described with this model. The results correlate with the experimental values for both permittivity and piezoelectric constants in the poling direction. Dielectric and piezoelectric properties were significantly improved with respect to randomly dispersed piezoelectric ceramic powder–polymer composites and the maximum g_{33} was shifted to a lower volume fraction. The results could have implications for development of dielectric and piezoelectric (nano-)fiber composites for dielectrics such as embedded capcitors, as well as piezoelectrics for sensing and energy harvesting applications. © *2012 American Institute of Physics*. [http://dx.doi.org/10.1063/1.4729814]

INTRODUCTION

Piezoelectric materials are used in many applications as sensing actuating or energy harvesting elements. Piezoelectric ceramics possess excellent electromechanical coupling coefficients but suffer from high density, poor mechanical properties, and difficult processing. Many attempts have been made to incorporate a piezoelectric ceramic phase in a polymer matrix, where the connectivity of both phases plays a major role in influencing the above mentioned aspects.[1] For instance, conventional 1–3 composites can achieve higher coupling coefficients and voltage sensitivity than monolithic ceramics but are generally difficult to process. This results in costly materials that are less suitable for large scale cost effective manufacturing. Alternatively, low-cost composites such as 0–3 lead zirconate titanate (PZT) particle-polymer composites suffer from deprived piezoelectric properties compared to their 1–3 counterparts. This is due to limited connectivity and the mismatch in permittivity between the matrix and the piezoelectric inclusions.

Dielectrophoresis (DEP) is a process which allows *in situ* structuring of particles in composites via directed self assembly. Quasi 1-3 structures are formed from initially randomly oriented dielectric particles in a thermosetting resin. When an alternating electric field is applied during curing of the matrix, the dielectric particles coalesce to form chains, oriented in the direction of the applied field.[2,3] Several potential applications have been proposed, such as temperature sensors,[4] dielectrics for embedded capacitors,[3,5] and piezoelectric elements for energy harvesting.[6]

It has been shown recently that the alignment of PZT equiaxed granulate particles in an epoxy resin results in an improvement of the piezoelectric properties over 0–3 composites with randomly dispersed particles. The improvement is especially apparent at low PZT volume fractions.[7] The ratio of particle size over inter particle distance, $R = \frac{l_2}{l_1}$, in the oriented particle chains dictates the enhancement of the piezoelectric effect. However, the properties of the particle based composites are still relatively low. This is because the maximum R that can be obtained is limited due to particle geometry. The minimum inter particle distance due to roughness and irregular shape is significant compared to particle dimension in the field direction.[7,8] The R value can be increased by aligning particles with an aspect ratio (AR) higher than one.[8] The particle aspect ratio is defined as the longest axis over the shortest axis, $AR = \frac{c}{a}$. However, it is also known that full alignment of large aspect ratio particles may be more difficult to achieve than it is for smaller aspect ratio particles when starting from a randomly oriented dispersion.[9]

In this paper, the results are presented of *in situ* 2D alignment studies of short fibers. The influence of aspect ratio on the final orientation distribution is studied. The dielectric and piezoelectric properties of DEP aligned composites with

a)Author to whom correspondence should be addressed. Electronic mail: daan.vandenende@tno.nl.

different volume fractions are presented. The aspect ratio of the PZT particles is also varied. The dielectric and piezoelectric properties of the composites can be described by an analytical model. The model describes the oriented particles in the non-piezoelectric matrix as a series-parallel configuration. Furthermore, the theory which relates the aspect ratio of the particles and their average orientation to the electric field acting on the particles is presented. The theoretical predictions are correlated with experimentally determined values.

THEORY

The orientation of non-spherical particles in a dielectric fluid will influence the electric field acting on them.[10–12] Ignoring the influence of complex poling states in the PZT as a result of off-axis alignment of polarization in the short fibers, the short fiber particles in a continuous matrix can be approximated by treating them as homogeneous ellipsoidal inclusions, since the polarizability of a cylinder is close to that of an ellipsoid.[10] The depolarization factor, N, for homogeneous ellipsoid with semi-axes a, b, c in a uniform electric field is presented as[11,12]

$$N_i = \frac{abc}{2}\int_0^\infty \frac{ds}{(s+\alpha^2)\beta} \quad (\alpha = a, b, c), \tag{1}$$

where $\beta^2 = (s+a^2)(s+b^2)(s+c^2)$. For ellipsoids oriented with their long axis parallel to the electric field direction, $\alpha = a$. For prolate ellipsoids which are perfectly aligned in the direction of the electric field, closed form solutions to the integrals in Eq. (1) are available.[12] When the electric field direction is parallel to the z-axis, the depolarization factors become

$$N_z = \frac{1-e^2}{2e^3}\left(\ln\frac{1+e}{1-e} - 2e\right), \tag{2}$$

$$N_x = N_y = \frac{1}{2}(1-N_z), \tag{3}$$

where the eccentricity, e, is related to the aspect ratio of the particle, AR, by

$$e = \sqrt{1-{}^{a^2}/_{c^2}} = \sqrt{1-(AR)^{-2}}. \tag{4}$$

Dielectrophoresis dynamics

When a lossless, anisotropic particle in a dielectric fluid is subjected to an electric field, the particle will align itself in the direction of the applied field. The preferred orientation axis is the particle axis with the lowest depolarization factor.[12] For lossy particles and matrix, the complex depolarization factor is used[13] and the orientation axis of the ellipsoid becomes frequency dependent. The torque $\vec{T}$ acting on dipole, $\vec{\mu}$ in a uniform applied field, E_{app}, is equal to[14]:

$$\vec{T}_{DEP} = \vec{\mu} \times \vec{E}_{app}. \tag{5}$$

For in-plane electric field and rotation, Eq. (5) reduces to Eq. (6) (for rotation in the y-z plane)[14,15]:

$$T_{DEP} = \frac{-2\pi}{3} abc\varepsilon_0 (N_z - N_y)\mathrm{Re}(K_y^* K_z^*) {E_{app}}^2 \sin 2\theta, \tag{6}$$

where θ is the orientation angle, and the complex polarizability factor, K_i^*, is equal to[13]:

$$K_i^* = \frac{\varepsilon_2^* - \varepsilon_1^*}{3(\varepsilon_1^* + [\varepsilon_2^* - \varepsilon_1^*]N_i)} \text{ for } \quad i = y, z, \tag{7}$$

where $\varepsilon_2^* = \varepsilon_2' + j\varepsilon_2''$ is the complex permittivity of the ceramic and $\varepsilon_1^* = \varepsilon_1' + j\varepsilon_1''$ is the complex permittivity of the surrounding medium. Finally, the particle is assumed to be half submerged in the liquid (see the Results and Discussion sections for relevance of this assumption). Neglecting the influence of fringing fields, the total dielectrophoresis induced torque becomes $T_{DEP} = \frac{T_{DEP,liquid} + T_{DEP,air}}{2}$.

The hydrodynamic drag induced torque is equal to[18]:

$$T_{drag} = (f_b + f_s)c^3 \eta \omega, \tag{8}$$

where f_b and f_s are, respectively, the bulk and surface contributions to the drag coefficient; η is the effective viscosity of the liquid/air interface; and ω is the angular velocity. Again the particle is assumed to be half submerged leading to an effective viscosity of $\eta = \frac{\eta_{liquid} + \eta_{air}}{2}$. The interface viscosity is assumed to be negligible compared to bulk viscosity, which is not unreasonable for liquid surfaces[18] and only Marangoni forces are accounted for. In this situation, the Boussinesq number is assumed to be equal to zero. Thus, the surface contribution can be approximated by $f_s = \frac{\pi}{12}$.[18] The bulk contribution to the hydrodynamic drag torque is calculated for ellipsoidal inclusions using[15,16]

$$f_b = \frac{8\pi ab(a^2+b^2)}{3c^2(a^2 N_z + b^2 N_y)}. \tag{9}$$

When treating the inclusions as slender rods, this contribution can be approximated by[17]

$$f_b = \frac{\pi}{\ln(2c'/b') - 0.8} \tag{10}$$

with c' equal to half the length of the rod and b' is the rod radius.

Finally, inertia induced torque acting on an ellipsoid rotating around its geometric centre is equal to

$$T_{inertia} = \frac{4\pi}{15}\rho abc(a^2+b^2)\alpha, \tag{11}$$

where ρ is the density of the ellipsoidal particle and α is the angular acceleration. By solving the equation $T_{DEP} = T_{drag} + T_{inertia}$, the kinetics of the DEP induced rotation can be determined.[15] This second order differential equation can be

simplified by neglecting the inertia term, which is found to be several orders of magnitude smaller than the remaining terms for the system under the conditions studied here.

Translational motion of the particles is caused by the dielectrophoresis force, which is non-zero in a non-uniform electric field. The dielectrophoresis force, $\vec{F}_{DEP}$, acting on a dipole is proportional to[14]

$$\vec{F}_{DEP} = (\vec{\mu} \cdot \nabla)\vec{E}_{app}. \tag{12}$$

Local non-uniformity of the electric field is caused by polarization of particles in a fluid. A single particle will experience a net force due to distortions caused by other particles in its vicinity. The magnitude of the distortions is proportional to the distance between the neighboring particles. This force will cause directed self assembly of the fibers, causing them to dynamically cluster under the application of the field.

Aligned ellipsoidal particles in composites

In the dilute limit, the relative electric field, Γ_{AR}, acting on an ellipsoidal inclusion with aspect ratio *AR* oriented in the electric field direction (i.e., the z-direction in Figure 1) is given by[10–12]

$$\Gamma_{AR} = \frac{E_{2,dilute}}{E_{app}} = \frac{\varepsilon_1}{\varepsilon_1 + N_z(\varepsilon_2 - \varepsilon_1)}. \tag{13}$$

Equation (13) states that the relative electric field acting on the inclusion increases with decreasing depolarization factor in the direction of the electric field. The depolarization factor is low for high aspect ratio particles (see Eqs. (1)–(4)). The higher electric field acting on the particles will increase the particle contribution to the permittivity and piezoelectric constants of the composite.[12] Several micromechanics models have been devised which take high aspect ratio particle inclusions into account. These models are based on the calculation of effective electroeleastic moduli, by substituting equivalent electroelastic Eshelby tensors in a model for finite concentrations of these inclusions, such as Mori-Tanaka approaches.[19–22] Finite element method (FEM) approaches have also been explored.[20,22] However, these studies have all considered equidistant spacing of the piezoelectric particles in the matrix as a function of volume fraction, a condition that is not satisfied by the DEP processed composites, as the dielectric particles tend to align end-to-end during the processing. Thus, even at low concentrations, aligned particles are still in close proximity of each other.

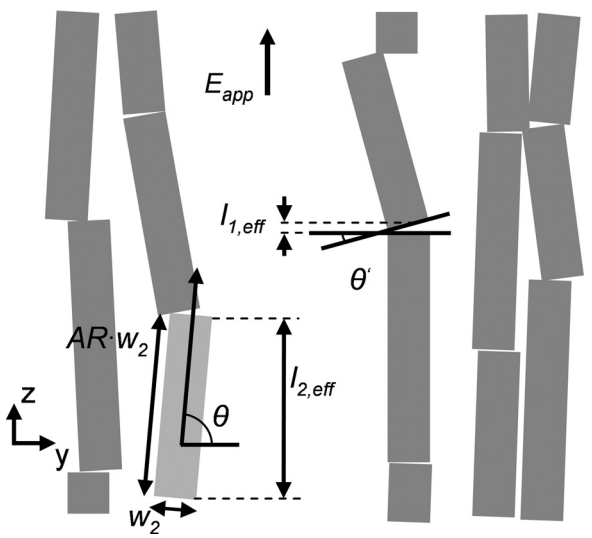

FIG. 1. Schematic of a cross section of the aligned fibers including the particle dimensions, w_2, AR and orientation angle, θ and the difference in angle between 2 fibers, θ'. For this schematic cross section, the average values are $\tilde{\theta} = 85.5°$ and $\tilde{\theta}' = 4.1°$.

The series-parallel model for dielectric properties of structured piezoelectric composites, introduced by Bowen *et al.*,[8] assumes perfectly intact chains of particles with equidistant spacing. This modification of the well known mixing rule for 1–3 composites includes a specific particle spacing parameter and has been adapted for piezoelectric properties of these materials.[7] When the particles are in close proximity to each other, interaction between the particles occurs. By treating the particle and matrix as 2 capacitors connected in series (i.e., effects of finite lateral dimensions are not taken into account), the relative electric field acting on the particle, Γ_S, can be calculated using the size ratio of the particle length over the inter particle distance, $R = \frac{l_2}{l_1}$.[8] For aligned ellipsoidal particles, $l_2 = 2c$.

$$\Gamma_s = \frac{E_{2,series}}{E_{app}} = \frac{(1+R)\varepsilon_1}{\varepsilon_2 + R\varepsilon_1}. \tag{14}$$

The equations for permittivity, ε_{DEP}, and piezoelectric charge constant, $d_{33_{DEP}}$, according to this model[7,8] are presented in Eqs. (15) and (16):

$$\varepsilon_{DEP} = \varphi\left[\frac{R\varepsilon_1\varepsilon_2}{\varepsilon_2 + R\varepsilon_1}\right] + (1-\varphi)\varepsilon_1, \tag{15}$$

$$d_{33_{DEP}} = \left[\frac{\varphi s_1}{\varphi s_1 + (1-\varphi)s'_{33_2}}\right]\left[\frac{(1+R)\varepsilon_1}{\varepsilon_2 + R\varepsilon_1}\right] d_{33_2}, \tag{16}$$

where φ is the PZT volume fraction; s_1 and s_{33_2} are, respectively, the compliances of the (isotropic) polymer and ceramic inclusions; s'_{33_2} is the equivalent compliance of the chains; and d_{33_2} is the piezoelectric charge constant of the ceramic inclusions.

However, this model does not include a particle shape or orientation parameter and is only suitable for ideally aligned particles with aspect ratio close to one. The ratio of particle size to inter particle distance, R, must be adapted to account for non-ideal alignment of non-equiaxed particles. Both aspect ratio related and series configuration related effects can be combined to approximate the solution for the ratio of electric field acting on an aligned chain of high aspect ratio particles by combining Eqs. (13) and (14). Since both equations converge to $\frac{E_2}{E_{app}} = 1$, the combined situation must also. This condition is satisfied if the series contribution decreases as the aspect ratio increases. A possible relation for this combined contribution is

$$\Gamma = \frac{E_2}{E_{app}} = \Gamma_{AR} + (1 - \Gamma_{AR})\Gamma_s. \tag{17}$$

This relation converges to $\frac{E_2}{E_{app}} = 1$ for infinitely long particles with infinitesimal spacing, which is consistent with the relation for 1–3 composites.

For a DEP structured composite, the fibers are likely to be non-ideally aligned (see Figure 1). The orientation angle of the particles in the composites, θ, is defined as the angle between the particle long axis and the electrode plane and θ' is the angle between the long axes of 2 adjacent particles. The model uses average values for the orientation angles, $\tilde{\theta}$ and $\tilde{\theta}'$, which are substituted place of θ and θ' to calculate the effective properties of the piezoelectric phase. The average angle difference between the particles, $\tilde{\theta}'$, is defined as equal to one standard deviation of the distribution of particle angles. The effective particle aspect ratio in the direction of the applied electric field can be approximated by decomposing the particle dimensions along the different axes. If the contribution perpendicular to the electric field is neglected, the effective aspect ratio can be approximated by

$$AR_{eff} = \Big(1 + \sin\theta(AR - 1)\Big), \tag{18}$$

which reduces to an effective AR of 1 for fibers aligned parallel to the applied field. Equation (4) then becomes

$$e_{eff} = \sqrt{1 - (1 + \sin\theta(AR - 1))^{-2}}, \tag{19}$$

which can be used to calculate the effective depolarization factor, $N_{z,eff}$, using Eq. (2). The effective particle size in the field direction now becomes

$$l_{2,eff} = w_2\Big(1 + \sin\theta(AR - 1)\Big), \tag{20}$$

where $l_{2,eff}$ is the effective particle dimension in the direction of the applied field, θ is the angle of orientation of the particles within the composite ($\theta = 90°$ is defined as aligned parallel to the electric field direction) and w_2 is the diameter of the particle cross section.

The inter particle distance can also be related to microstructure. If all particles are perfectly oriented and aligned end-to-end in the direction of the electric field, the inter particle distance will be at a minimum, and in the order of the particle surface roughness, R_a. However, when the particles are on average not oriented perfectly along the axis of the applied electric field, the average inter particle distance will increase according to the difference in alignment between both particles, the angle θ' (see Figure 1).

$$l_{1,eff} = R_a + C\sin\theta'\frac{w_2}{2}, \tag{21}$$

where C is a constant related to the properties of the interface between the fibers. By combining Eqs. (20) and (21), the effective particle ratio, R_{eff}, now becomes

$$R_{eff} = \frac{1 + \sin\theta(AR - 1)}{\frac{R_a}{w_2} + \frac{C\sin\theta'}{2}}. \tag{22}$$

From Eqs. (21) and (22), it can be seen that the surface roughness of the particles also serves as a first order estimate for the minimum achievable inter-particle distance, which governs the upper limit of the composite properties. When all particles are perfectly aligned, $\tilde{\theta} = 90°$ and $\tilde{\theta}' = 0°$, Eq. (22) reduces to

$$R_{eff} = \frac{l_{2,eff}}{l_{1,eff}} = \frac{w_2 AR}{R_a}. \tag{23}$$

By using Eq. (19) instead of Eq. (4) for calculating Eqs. (2) and (3) and Eq. (22) in place of Eq. (14) and substituting $\tilde{\theta}$ and $\tilde{\theta}'$ for θ' and θ, the effective ratio of the electric field acting on the particle, Γ_{eff}, can be calculated using Eq. (17) as

$$\Gamma_{eff} = 1 - \frac{\Big(N_{z,eff}(\varepsilon_2 - \varepsilon_1)^2\Big)}{(\varepsilon_2 + R_{eff}\varepsilon_1)\Big(\varepsilon_1 + N_{z,eff}(\varepsilon_2 - \varepsilon_1)\Big)}. \tag{24}$$

The equations for permittivity and piezoelectric charge constants of non-ideally aligned high aspect ratio particle composites can now be described with the following equations:

$$\varepsilon_{DEP} = \varphi\left[\frac{(\Gamma_{eff}\varepsilon_2 - \varepsilon_1)\varepsilon_2}{(\varepsilon_2 - \varepsilon_1)} - (\Gamma_{eff}d_{33_2})^2\frac{1 - \varphi}{\varphi s_1 + (1 - \varphi)s'_{33_2}}\right] + (1 - \varphi)\varepsilon_1, \tag{25}$$

$$d_{33_{DEP}} = \left[\frac{\varphi s_1}{\varphi s_1 + (1 - \varphi)s'_{33_2}}\right]\Gamma_{eff}d_{33_2}. \tag{26}$$

In Eq. (25), the clamping effect caused by the d_{33} of the poled fiber inclusions is included. Hence for $\Gamma_{eff}=1$ and $s'_{33_2} = s_{33_2}$, these equations are equal to the equations for 1–3 composites.[23]

EXPERIMENTAL

Composites manufacturing

PZT fibers were manufactured by wet spinning technique. PZT particles (PZT5A4, Morgan Electroceramics, Ruabon, UK) were mixed in a 25 wt. % solution of cellulose acetate (Mw. 100 000; Acros Organics) in acetone with a PZT-cellulose acetate volume ratio of 2:3 and spun in a water coagulation bath. The PZT green fibers were dried and subsequently sintered for 1 h at 1200 °C in air in a closed Al_2O_3 crucible. Typical fiber cross sectional dimensions were approximately $l \times w = 20\,\mu m \times 40\mu m$. Typical surface roughness of the fibers was measured to be $R_a = 0.42\,\mu m$ (for a length scale equal to the fiber width) using a confocal microscope (Sensofar plμ2300). Sintered fibers were

manually broken and different aspect ratio short fibers were roughly separated by sieving through sieves with different mesh sizes. Appropriate amounts of PZT fibers were mixed with a room temperature curing, two component polyurethane (PU) resin (Crystal Clear 202, Smooth-on Inc., Easton, USA). The properties of the matrix resin were measured to be $\eta = 600$ mPas, $\varepsilon^*/\varepsilon_0 = 5.13 + j3.76$ (100 Hz, start of cure), and $s = 6.25 \times 10^{-10}\text{Pa}^{-1}$ (flexural mode), $\varepsilon^*/\varepsilon_0 = 3.26 + j0.064$ (1 kHz, fully cured). After mixing, the composite resin was drawn into a pipette and immediately deposited in an open PMMA container with copper tape electrodes attached on both sides (see Figure 2). A signal generator (Tektronix AFG320) was coupled to a high voltage amplifier (Trek Model 610-A) for applying the electric field. The electric field was switched on directly after deposition of the composite mixture to avoid settling of the short fibers. The applied structuring electric fields ranged from 0.5 kV/mm to 4 kV/mm and was considered across this range to achieve different levels of alignment. After post-curing at 75 °C for 4 h, gold electrodes were sputtered on both sides of the composites. The samples were subsequently poled at 8 kV/mm at 90 °C in a silicone oil bath for 30 min. The poling field was removed after cooling back to room temperature.

As a reference, 1–3 composites were manufactured by embedding as sintered fibers in PU in heat shrink plastic tube and cured at 65 °C. After sintering, the fibers were aligned but relatively loosely packed and the PU resin could infiltrate the fibers. During curing of the PU resin, the heat shrink tubing shrinks and compacts the fibers leading to higher final PZT volume fractions. After post-curing at 75 °C, the 1–3 composites were sliced and polished to the desired thickness and gold electrodes were sputtered on both sides.

Alignment kinetics analysis

The PMMA container was filled completely with one of PU components (part B, resin, $\eta = 350$ mPas, $\varepsilon_1^*/\varepsilon_0 = 10.2 + j9.76$ (300 Hz)). PZT short fibers were deposited on the surface of the PU. The surface tension of the PU keeps the fibers on the surface of the liquid. The fibers were held on the surface by the surface tension of the PU resin. A structuring field of 0.5-2 kV/mm was applied while recording the images of the PZT fibers with an optical microscope (Zeiss Axioscope). Orientation distributions of the fibers and average length of the chains of fibers after various intervals were obtained using the software ImageJ.

Materials characterization

Complex permittivity of the polyurethane resin and unpoled PZT5A4 ceramics were measured for $f = 20$ Hz-1 MHz using an HP 4284 A LCR meter and for $f = 1$ Hz-20 Hz using an Iviumstat xr impedance analyzer (Ivium Technologies, Eindhoven, The Netherlands). Permittivity of the cured composites was measured at a fixed frequency of $f = 1$ kHz. Finally, d_{33} measurements were performed with a Berlincourt type d_{33} meter (PM3000, PiezoTest, UK) with flat electrodes to obtain an average d_{33} across the sample. After piezoelectric characterization, optical micrographs of the composites cross sections were analyzed to assess the average orientation of the short fibers in the composites. Per sample, 4 micrographs were taken at different depths of the composite and image analysis using the software ImageJ was used to obtain the average orientation angle of the fibers using the method described in Ref. 7. For several samples, a 3D x-ray tomography image (Phoenix X-ray Nonotom S) was made for comparison. For the scan, three images were taken and averaged per 0.5° of rotation for a full revolution scan. Finally, the PU matrix was burnt off to free the PZT fibers. Fibers were dispersed on a flat plate and optical micrographs were taken. The length and width of each of the individual fibers were obtained using ImageJ software. From these measurements, the volume weighted average aspect ratio was calculated for each sample.

RESULTS

Single fiber rotation

The rotation behavior of particles with aspect ratios higher than one was found to be frequency dependent. In Figure 3, the measured maximum angular velocity as a function of frequency is compared to the real part of the complex polarizability factor of the particle (see Eq. (6)). In all experiments, the particles were initially oriented perpendicular to the direction of the electric field, except during the experiment at $f = 5$ Hz, where the particle was initially oriented parallel to the field direction. In Figure 3, rotation

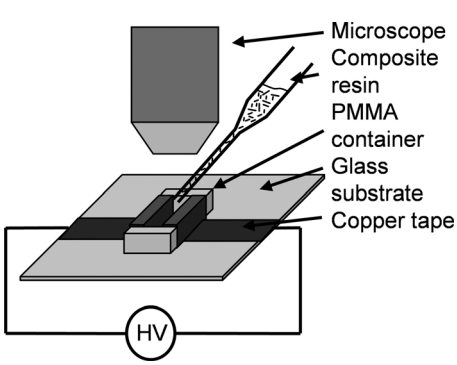

FIG. 2. Schematic of the setup used to align the PZT short fibers in the composite resin.

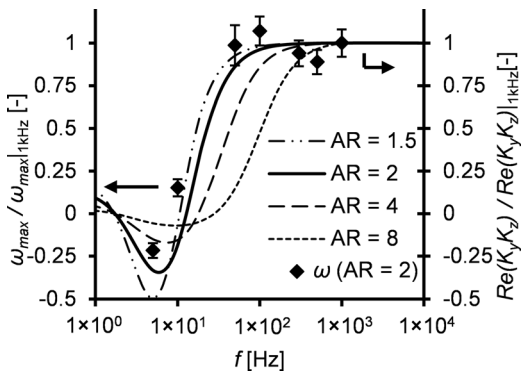

FIG. 3. Frequency dependence of the maximum angular velocity compared to the real part of the complex polarization factor. The values relative to the value for f = 1 kHz are plotted for both $\omega_{\max}$ and $\text{Re}(K_y^* K_z^*)$, respectively.

towards alignment in the direction of the electric field is defined as positive angular rotation, irrespective of whether the rotation is clockwise or not. Both clockwise and counter clockwise rotations were witnessed during experiments.

In Figure 4, the maximum angular velocity of a particle with AR = 2 as a function of applied electric field is presented. The theoretical predictions correlate well to the measured values up to $E_{app} = 0.75$ kV/mm. At $E_{app} = 1$ kV/mm, the measured value is slightly lower than the predicted maximum angular velocity using both Jeffery's and Burgers' equations for hydrodynamic torque (Eqs. (9) and (10)).

Alignment of multiple fibers

A snapshot of typical dielectrophoretic alignment is presented in Figure 5. The snapshots show that individual particles which are free to rotate orient in the direction of the electric field within seconds. In more complex configurations of particles, individual particles may remain at off-axis orientations for longer periods of time. With time, individual particles connect to form chains. Chains which are free to move (i.e., not bound to one of the electrodes) are attracted towards other chains during later stages of the dielectrophoresis process; a phenomenon seen before in DEP processed composites.[24]

The average orientation angle $\tilde{\theta}$ and relative average chain length, $\frac{\tilde{L}}{L_{max}}$, as a function of time for a typical experiment are represented in Figure 6. Here, L_{max} is defined as the length of the microscope image in the direction of the electric field. The volume fraction was determined at the start of the experiment using image analysis methods. Time constants τ_L and τ_ω were calculated for translation and rotation of the particles, respectively, by determining the time at which the orientation angle or chain length reaches a value of $1 - 1/e \approx 0.632$ relative to the final value, i.e., when geometric reorientation of fibers no longer takes place. The chain length value for volume fraction, $\varphi_{2d} = 0.025$ was extrapolated from the experimental curve as no stable situation was reached within the recording time. The values for τ_L and τ_ω as a function of volume fraction, φ_{2d}, are presented in Figure 7. Above volume fractions of $\varphi_{2d} = 0.15$, no reliable chain length data could be measured as all particles are interconnected from the start of the experiment and remain connected even during rotation of individual particles upon applying the electric field.

In Figure 8, the orientation angle of individual fibers inside polymer chains is presented as a function of aspect ratio. Each data point is an average value of 5 measured points of equal aspect ratio. The chains investigated were free standing and had a single particle width to avoid complication of lateral interactions of multiple fibers. Lower aspect ratio particles were found to be less aligned, frequently being

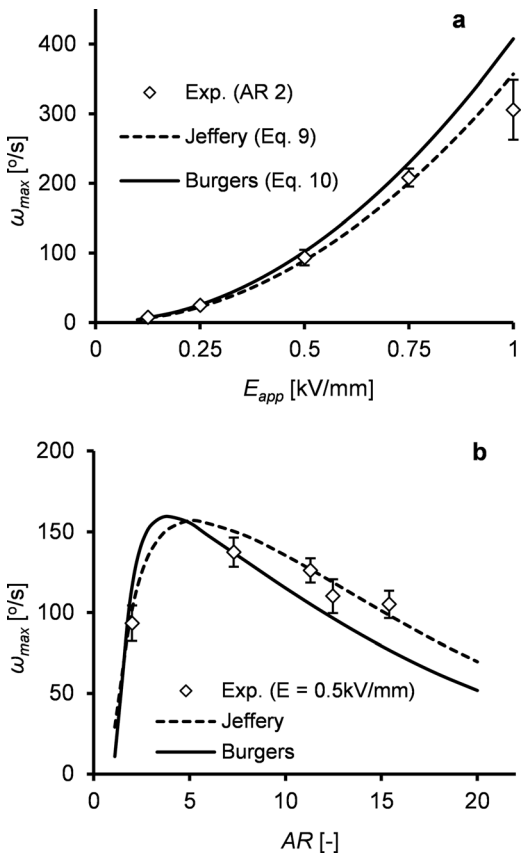

FIG. 4. Maximum measured angular velocity as a function of particle aspect ratio at a fixed applied electric field of $E_{app} = 0.5$ kV/mm compared to theoretical predictions using equations of Jeffery (Eq. (9)) and Burgers (Eq. (10)) for hydrodynamic drag induced torque (a). Maximum angular velocity as a function of aspect ratio of the particles (b).

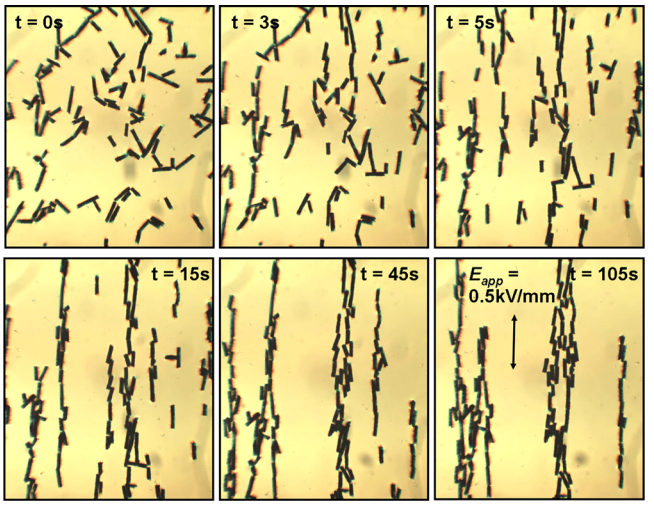

FIG. 5. Snapshots at various times during DEP alignment in a structuring field of 0.5 kV/mm for a composite mixture with PZT concentration of $\varphi_{2d} = 0.09$.

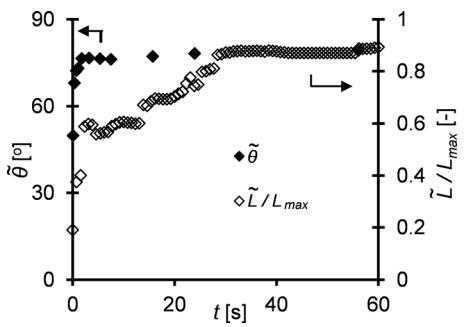

FIG. 6. Typical evolution of average orientation angle $\tilde{\theta}$ and average chain length $\tilde{L}$ of particles over time. Conditions are $E_{app} = 0.5$ kV/mm, $f = 300$ Hz, $\varphi_{2d} = 0.11$, and average AR = 6.

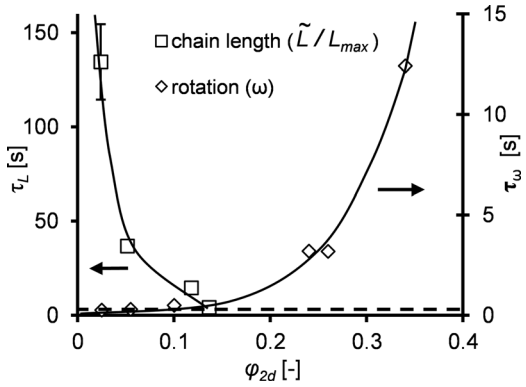

FIG. 7. Time constants for rotation and chain formation for different volume fractions of particles. Experimental conditions are $E_{app} = 0.5$ kV/mm, $f = 300$ Hz, $\varphi_{2d} = 0.11$, and average AR = 6. Note the scale difference between the τ_L and τ_ω axes. The dotted line represents the rotation time constant for a single particle of similar *AR*.

connected to an adjacent particle corner to corner, causing the final particle orientation to be off-axis. The effect has been witnessed before in aligned particle and short fiber composites.[25]

The effect of electric field on the orientation of particles with different aspect ratios is presented in Figure 9. The average orientation angle, $\tilde{\theta}$, and the spread in orientation angles, $\tilde{\theta}'$ (defined as one standard deviation of the orientation distribution) are shown to decrease with electric field. After a processing time of 50 s (i.e., longer than 5 times the representative time constants for a volume fraction of $\varphi_{2d} = 0.25$), little difference between the particles of different aspect ratios is witnessed.

In Figure 10, the average orientation of fibers in the liquid PU resin is qualitatively compared to the orientation of fibers in the cured composites for volume fractions up to $\varphi_{2d} = 0.35$.

Microstructure of DEP processed composites after curing

In Figure 11, the typical microstructures of DEP processed composites are presented. The PZT particles are predominantly oriented in the direction of the electric field. A small fraction of the particles are oriented perpendicular to the electric field, bridging neighboring particle chains as shown in Figure 11 (left side). In the right side of Figure 11,

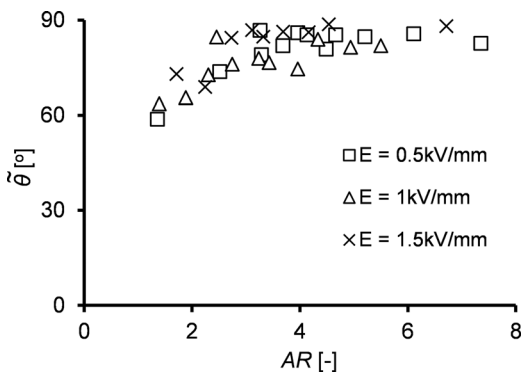

FIG. 8. Orientation angle θ of individual particles in aligned chains as a function of particle aspect ratio.

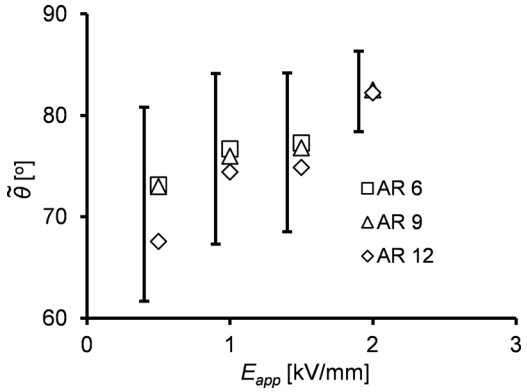

FIG. 9. Average orientation angle $\tilde{\theta}$ of particles as a function applied field of E_{app} at a time of $t = 50$ s, f = 300 Hz, and $\varphi_{2d} = 0.25$. The bars depict the standard deviation of the orientation distribution at each measured electric field.

a polished cross section is imaged. From these cross sections, the average orientation factor of the cured composites can be determined. In Figure 12, a three dimensional tomographic image of the oriented PZT fibers is presented. Most of the fibers are well aligned in the direction of the applied field. However, in several regions, for instance in the centre of the composite, a region with lower average orientation is located. The physical origin of such local misalignments is addressed in the discussion. Nevertheless, a maximum difference in average orientation angle of only 2.65° was measured between 12 cross sections at different positions in the sample. The average orientation angle calculated using CT cross sections was $\tilde{\theta} = 73.6° \pm 0.7°$ (8 cross sections). The average angle for optical microscopy cross sections was $\tilde{\theta} = 74.3° \pm 0.6°$ (4 cross sections).

Piezoelectric and dielectric properties

1–3 composites

The dielectric and piezoelectric properties as a function of PZT volume fraction of reference composites with full 1–3 connectivity are presented in Figure 13.

The effective properties for ε_2 and $d_{33,2}$ were determined by fitting with least squares method using Eqs. (25) and (26),

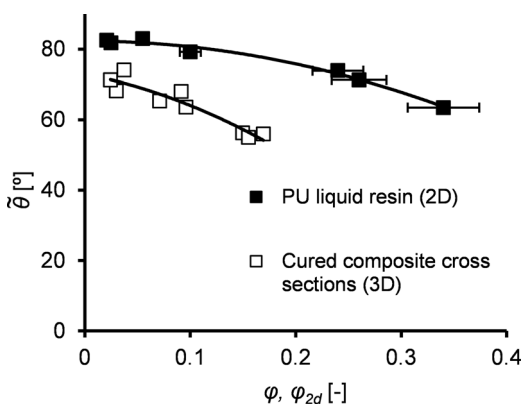

FIG. 10. Average orientation angles of particles in structuring experiments (2D) as a function of φ_{2d} ($E_{app} = 0.5$ kV/mm, $f = 300$ Hz) compared to angles of particles in cured composites as a function of φ ($E_{app} = 1$ kV/mm, $f = 100$ Hz). Particles with aspect ratio of $AR = 6$ were compared.

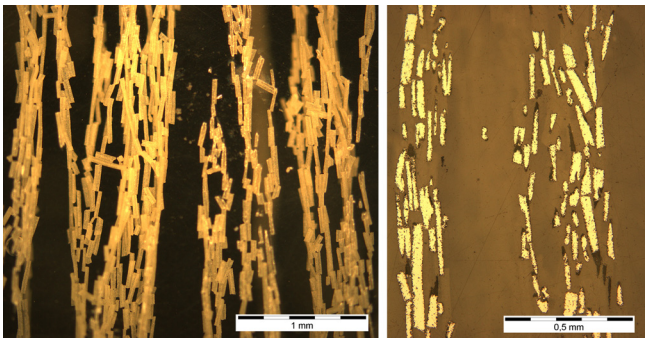

FIG. 11. Dark field optical image of a DEP processed PZT-PU composite ($\varphi = 0.03$, $AR = 7.2$, $\tilde{\theta} = 78.8°$) (left) and a bright field image of a composite cross section ($\varphi = 0.13$, $AR = 8.4$, $\tilde{\theta} = 74.7°$) (right).

with $\Gamma_{eff} = 1$ and $s'_{33_2} = s_{33_2}$. Values of $\varepsilon_2' = 1547$ and $d_{33,2} = 399$ pC/N were obtained. These properties are comparable to the values reported in literature for PZT5A fibers[26] and are used in the calculations of properties for DEP aligned 0–3 composites.

DEP aligned 0–3 composites

The dielectric and piezoelectric properties of composites as a function of PZT volume fraction of composites with different AR_{eff} are presented in Figures 14(a) and 14(b). The corresponding curves are modeled using Eqs. (25) and (26) using the corresponding values for Γ_{eff}. The exact relation between AR_{eff} and Γ_{eff} is described in detail in the Discussion section (see also Figure 17). The piezoelectric voltage constant g_{33} was calculated using the relation $g_{33} = \frac{d_{33}}{\varepsilon_0 \varepsilon_{33}}$ (see Figure 14(c)).

DISCUSSION

Alignment analysis

The torque acting on PZT fibers with aspect ratio $AR > 1$ is frequency dependent via the complex polarizability factor. The real part of this factor is known to depend on

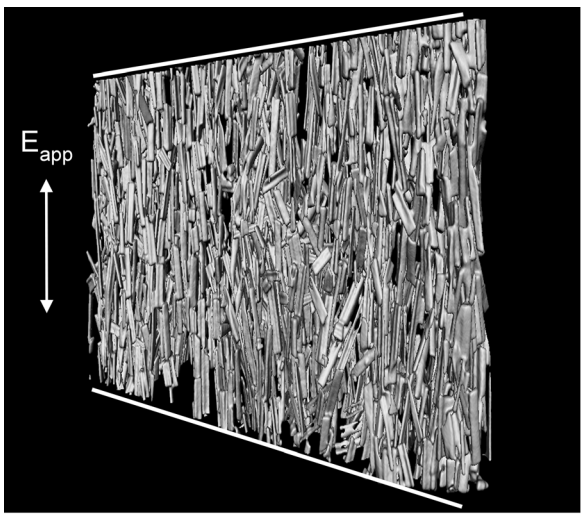

FIG. 12. 3D tomography image of DEP aligned sample containing 13 vol. % PZT short fibers in PU matrix. Only the PZT phase is represented. It is clear that the fibers are well aligned in the direction of the electric field ($\varphi = 0.13$, $AR = 8.4$, $\tilde{\theta} = 73.6°$).

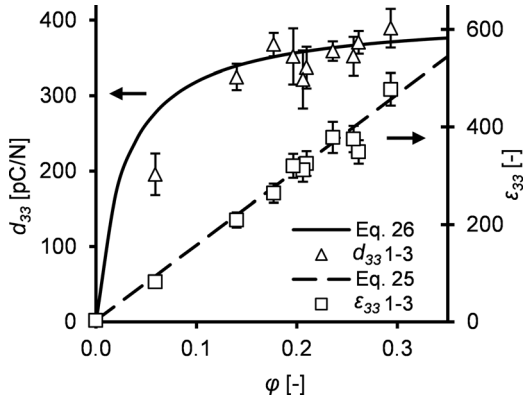

FIG. 13. Relative permittivity and piezoelectric charge constants of the 1–3 composites as a function of particle volume fraction compared to model values using Eqs. (24) and (25), respectively, with $\Gamma_{eff} = 1$.

the aspect ratio of the particles. For higher aspect ratio particles, the magnitude of the real part of the polarizability factor increases but so does the turnover frequency. *Ceteris paribus*, the sign and magnitude of this factor control the direction and speed of rotation of the particles[14] as can be seen in Figure 3.

The dieletrophoretic torque can be increased by increasing the electric field (Eq. (6)), resulting in a higher angular velocity. In Figure 4(a), the maximum angular velocity as a function of electric field is presented for a particle with aspect ratio $AR = 2$. The maximum angular velocity at this aspect ratio is well described when using Jeffery's equation for the hydrodynamic torque, indicating that the assumption of a half-submerged particle is realistic. At high electric fields, the measured angular velocity is slightly lower than predicted. This is possibly because at high fields the out of plane DEP force becomes significant. The result is that the particle will be pulled into the liquid. The relative increase in drag due to this is higher than the increase in DEP torque. This results in a progressively lower angular velocity with fraction of the particle that is submerged.

The particle aspect ratio also influences the alignment speed. For the particle-matrix combination studied here, the angular velocity reaches a maximum for particles with an aspect ratio of about 4 to 5 (see Figure 4(b)). Larger particles take longer to rotate. For even higher aspect ratios, the angular velocity logarithmically declines with AR. For instance, at an aspect ratio of $AR = 100$, the predicted maximum angular velocity will reduce to just $\omega_{max} \approx 13°/s$. At these high aspect ratios, however, the particles can no longer be treated as rigid. Bending and twisting may become significant. This will influence the speed of alignment.

In processing, the particle torque will contribute to alignment. At a fixed electric field, the speed at which particles orient is a function of volume fraction (Figure 7). The time constant τ_ω increases with volume fraction. The amount of fibers which are free to rotate without contacting neighboring particles will decrease when the fiber volume fraction increases. This leads to a slower, more complex pattern of reorientations at higher volume fractions. Also the final average orientation angle after stabilization is found to decrease with increasing volume fraction. This result is consistent

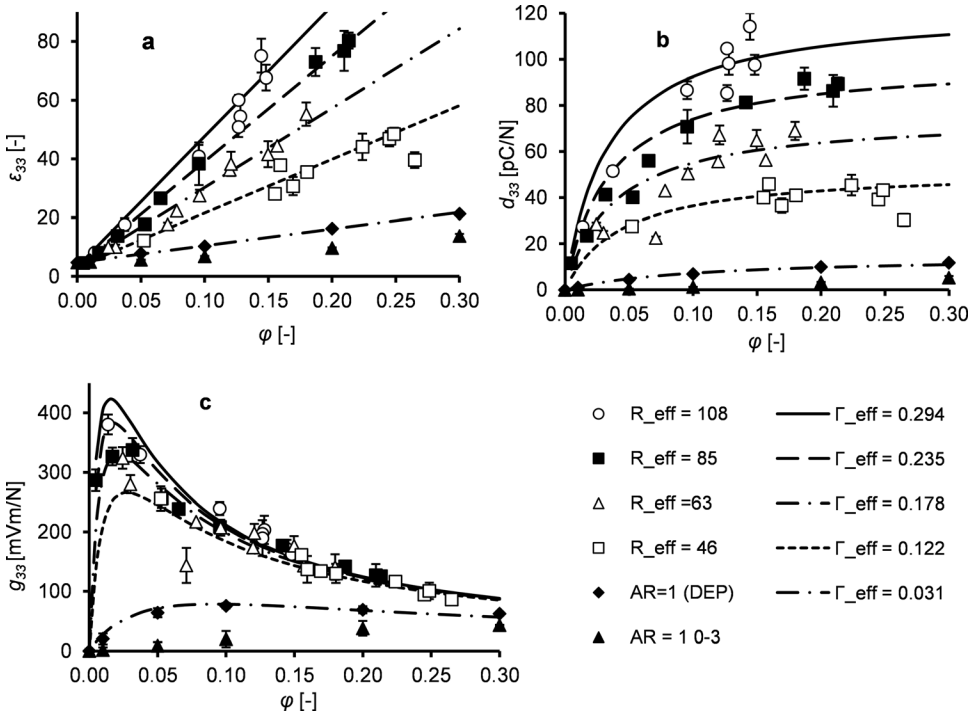

FIG. 14. Relative permittivity (a), piezoelectric charge constants (b), and piezoelectric voltage constants (c) in 33 direction of dielectrophoretically aligned composites as a function of particle volume fraction for different R_{eff} compared to model values using Eqs. (25) and (26), respectively. The values for particle composites (AR = 1) were taken from Ref. 7.

with previous observations in composites with short fibers aligned by external force fields.[9] The increase in the amount of fibers increases the number of contact points between fibers. At the edges and corners of the particles where adjacent particles are (almost) contacting, local gradients in electric field can become large. This leads to a more complex electric field pattern. This might cause the local direction of the electric field to be off-axis, which hinders alignment of the particles by torque induced rotation. At high fields, the PZT particles may even become (partly) poled. The poling could aid in fixating the fibers in off-axis positions. The effect is small for 2-dimensional alignment (Figure 9). It is more apparent for 3-dimensional alignment as can be seen in Figure 10. This is because the extra dimension increases the number of possible junctions between fibers. The effect of the electric field on alignment is quantified in Figure 9. The average alignment angle increases with the electric field magnitude for all aspect ratios studied. The increase is most apparent for the highest aspect ratio particles. This high orientation factor can be attributed to the fact that the particles are relatively free to move in the quasi 2-dimensional space because there is no rigid constraint for out of plane movement. The particles are only trapped at the interface via surface tension. Therefore, the large aspect ratio particles are able to slide over each other to when the torque acting on them is high enough. It was witnessed that fibers were not fully submerged when sliding over each other and emerged back on the surface of the fluid. In three-dimensional orientation, fibers are also free to rotate alongside each other. This may lead to surprisingly facile alignment of relatively large aspect ratio particles. This may be of importance for creating high aspect ratio nano-wire composites with a high degree of alignment. However, in the short fiber composites made in this study, the average orientation angle was significantly lower. As was stated, the greater number of degrees of freedom results in more contact points between particles. Second, the mixed resin and hardener has different properties than the resin (part B) only. The mixed viscosity is higher and the permittivity is lower, leading to lower DEP torque and forces. The second effect is matrix dependent and room for optimization exists. When particle chains are formed, the particles are predominantly aligned end-to-end. But low aspect ratio particles can remain rotated. This phenomenon is visible in the alignment videos as well as in cross sections of the cured composites (Figure 12). This final rotated position is also related to the dielectrophoresis force. The electric field gradient is thus highest at particle corners. Therefore, low AR particles will sometimes rotate to align point to point instead of face to face (see Figure 5). The torque acting on a particle increases when the particle is not fully aligned in the electric field direction (see Eq. (3)). This effect will counteract the rotation induced by the electric field concentration at the corners of the fibers. The dielectrophoresis induced torque is highly dependent on the aspect ratio of the fibers. The torque vanishes at $AR = 1$, when $N_z = N_y = 1/3$ which follows from Eqs. (4) and (6) (see also Figure 15). At a certain applied electric field, a minimum AR will be needed for the torque to overcome the possible corner-to-corner alignment of a particle inside a chain. For small AR particles, the torque is low and the particles are oriented at an angle (see Figure 8). The effect of applied electric field is low as the dependence of both T_{DEP} and F_{DEP} on electric field is proportional to E_{app}^2.[14,15]

For higher aspect ratio particles, the torque overcomes the dielectrophoresis force at the particle corners. Particle alignment parallel to the applied electric field is the result. This sometimes results in a staggered configuration of the particles (see Figures 5 and 11).

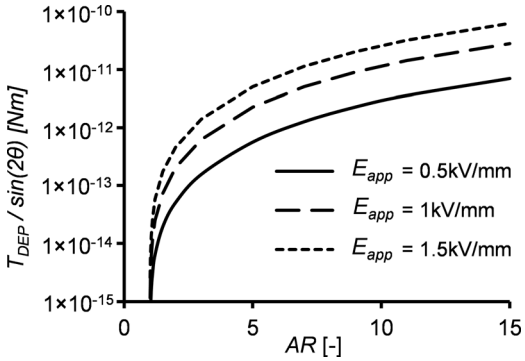

FIG. 15. Angle normalised torque as a function of aspect ratio of the particles for different applied electric fields.

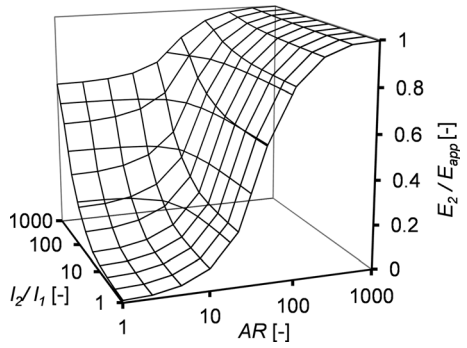

FIG. 17. Electric field ratio acting on an ellipsoidal PZT particle as a function of aspect ratio, *AR* and particle spacing, *R* using Eq. (17).

Relative electric field on the particles in a composite

The analytical results (Eq. (17)) for the ratio of electric field acting on an ellipsoidal PZT particle for a fixed relative permittivity values of $\varepsilon_1 = 3.26$ and $\varepsilon_2 = 1547$ are given in Figure 16. These results were compared to electric field distribution in a FEM model. The FEM results were calculated by analyzing a representative volume element (RVE). The RVE consists of 3 full cylindrical particles of aspect ratio *AR* and length l_2 and particles of length $l_2/2$ on both ends, all with spacing l_1. The average electric field was calculated in the middle particle and compared to the analytical results. The estimated ratio of electric field acting on the particles using Eq. (17) correlates extremely well with FEM modeling results for ellipsoidal particles. It indicates that the interaction between aspect ratio term and the parallel geometry term in Eq. (17) is well described for the current values of permittivity of both phases. The analytical results for the relative electric field acting on a particle as a function of both *AR* and *R* for fixed relative permittivity values of $\varepsilon_1 = 3.26$ and $\varepsilon_2 = 1547$ are presented in Figure 17. It is shown that for a particle aspect ratio of around 100, the electric field acting on the particle is close to $\Gamma = 1$ for this system. The relative permittivity values of both phases are representative for a typical PZT–polymer system. The result implies that for perfectly oriented particles with aspect ratios of around $AR = 100$ the electric field acting on the particles is close to the applied field. An aspect ratio of 100 is well within range

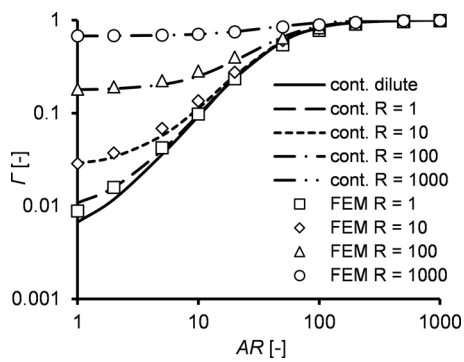

FIG. 16. Electric field ratio in a PZT particle as a function of aspect ratio, *AR*, for different particle spacing, *R*. FEM results are compared to results using Eq. (17).

of typical PZT nanowires.[27] This result indicates that apart from increasing the matrix permittivity, the aspect ratio of the inclusions can also be used to achieve higher permittivity and piezoelectric properties of the composite (see Eqs. (13) and (24)). For lower aspect ratio particle inclusions, a high electric field ratio is also achievable and helps increase both the dielectric constant and the energy density of the materials.[28] However, in this case careful attention must be paid to the average distance between the particles in addition to orientation only, depending on the application.

Permittivity and piezoelectric properties of the composites

The dielectric and piezoelectric properties of DEP aligned particles are presented in Figure 14 using piezoelectric constants for the PZT fibers obtained from 1–3 composites (see Figure 13). Using Eq. (22), samples with similar R_{eff} were selected. For the mean R_{eff}, the corresponding fitted value Γ_{eff} for these samples was calculated using Eq. (17). The calculated values correspond well to the measured samples. The maximum voltage constants for the DEP aligned materials are close to $g_{33} = 400$ mVm/N, which approaches the values for low φ 1–3 composites and is almost 15 times higher than bulk PZT5A4 ($g_{33} = 28$ mVm/N) and over 200 times the g_{33} value for 0–3 PZT epoxy composites at this volume fraction.[7] The maximum calculated values of g_{33} of a 1–3 composite occur at $\varphi = 0.007$ for the material parameters used in this study. However, these calculations assume isostrain conditions. Real values are known to deviate from this prediction due to non-ideal stress distributions between fiber and matrix.[29] This reduction in g_{33} is largest for extremely small volume fractions and quickly decreases at higher volume fractions.[30]

The R_{eff} values for all composite samples were calculated using Eq. (22). The distributions of orientation angles of short fibers within the DEP aligned composites were found to closely resemble a folded half normal distribution centered around $\theta = 90°$ and folded at $\theta = 0°$. For composite samples containing short fibers with different aspect ratios, the measured values for $\tilde{\theta}$, *AR* filled in Eq. (20) and the measured values for $\tilde{\theta}'$, R_a in Eq. (21). A representative value for the constant *C* in Eq. (21) was derived from the orientation distribution of the fibers (see Appendix) and was

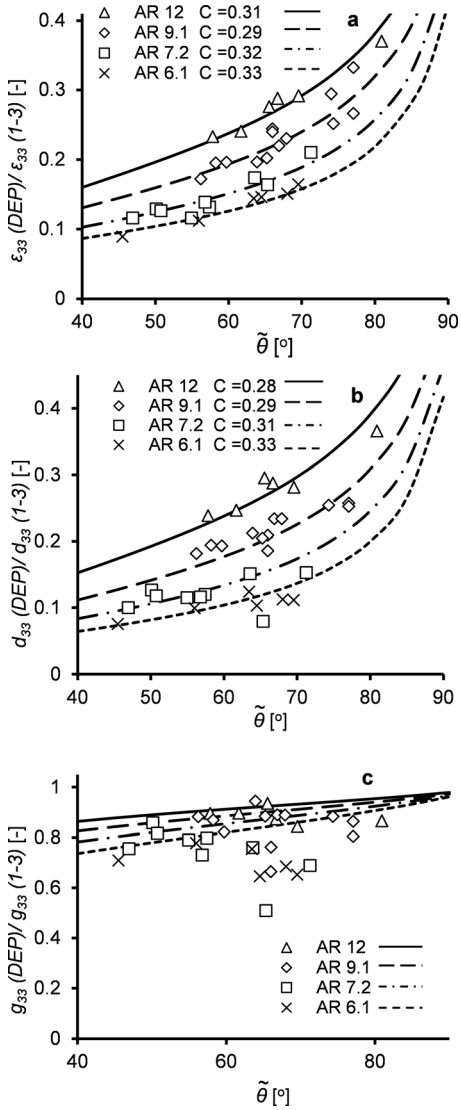

FIG. 18. Normalised permittivity (a), charge constants d_{33} (b), and voltage constants g_{33} (c) of the dielectrophoretically aligned composites with different aspect ratio particles as a function of $\tilde{\theta}$.

found to be $C = 0.404$. Subsequently, the relative ε_{33}, d_{33}, and g_{33} values are predicted using Eqs. (25) and (26). The normalized values are presented in Figure 18.

The permittivity and piezoelectric charge constants increase with particle aspect ratio and degree of alignment. The permittivity and piezoelectric properties of the composites with randomly oriented fibers are known to increase for high aspect ratio inclusions.[28,31–33] It has also been demonstrated that alignment of high aspect ratio particles increases the permittivity of the composite.[8,34,35] The calculated values correspond well with the experimental values of composites with low aspect ratios but tend to fall short for composites with higher aspect ratios. This is possibly due to the contribution of the large aspect ratio fibers. For large aspect ratio fibers, interactions between laterally contacting fibers may occur. These interactions can be accounted for in the model by the constant, C, in Eq. (21), which is a measure for the interaction between fibers. For higher aspect ratio fibers, the constant, C, must be reduced. Evidently, a region of overlap between fibers will yield a higher effective connectivity between two particles, which is reasonable. In mechanical sense, the coupling between adjacent fibers will increase by shear stress transfer between overlapping particles. Thus, the effect of overlapping particles is slightly larger for d_{33}, leading to a lower effective C. The validity of the model for very effective alignment has not verified due to lack of experimental samples with high orientations angles ($\tilde{\theta} > 80°$). The predicted values rise steeply when $\tilde{\theta}$ approaches 90°. However, precise values depend on the properties of the (nanoscale) interface between contacting fibers. The properties of the interface may differ from the bulk material values used in this work. When the inter particle distance becomes in the order of the surface roughness, the particle surface cannot be treated as flat and the precise electrical transfer depends on the effect that locally contacting grains in the fibers have on the dielectric transfer. The effective minimum l_1 value is then dependent on the real contact area between the two particles. Nevertheless, the model predictions indicate that there might be room for enormous improvement of the effective properties if alignment can be optimized.

The normalized ε_{33} and d_{33} values as a function of R_{eff} are presented in Figure 19. The measured values correlate well to the predicted values, though predicted values are slightly lower than the measured values for large values of R_{eff}. When the values are plotted against R_{eff} the relative values all fit to the same equation (Eq. (25)), irrespective of the differences in AR and $\tilde{\theta}$ values between the composites.

Other models for oriented high aspect ratio particles[21,22] assume uniform dispersion and orientation of the particles.

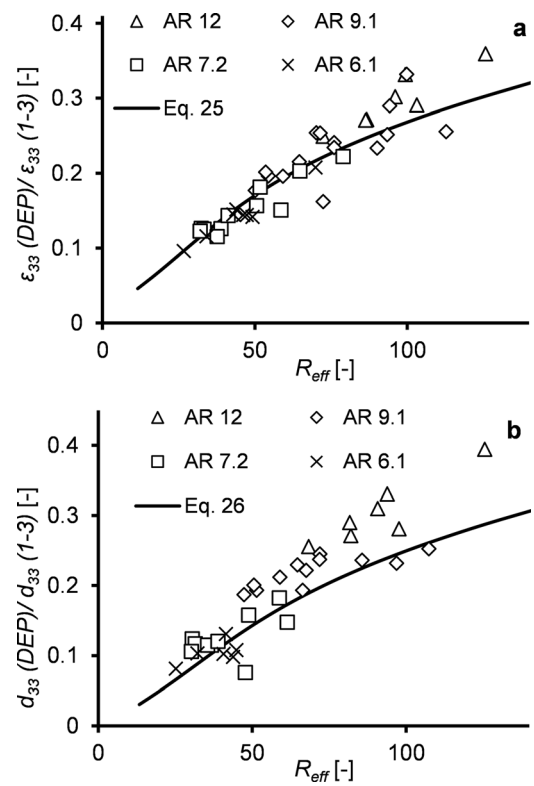

FIG. 19. Normalised measured permittivity ε_{33} (a) and piezoelectric charge constant d_{33} (b) of the dielectrophoretically aligned composites as a function of calculated R_{eff} for the samples compared to values calculated using Eqs. (25) and (26), respectively.

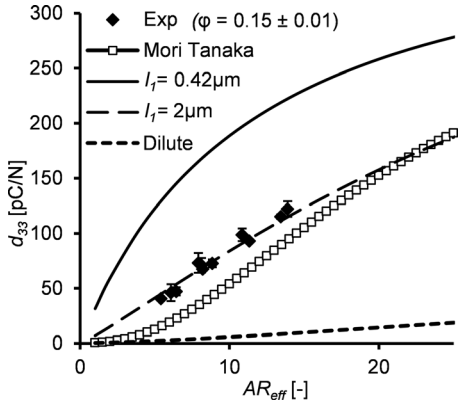

FIG. 20. Piezoelectric charge coefficients as a function of effective aspect ratio of the composites for $\varphi = 0.15$ compared to values predicted by various models. The inter particle distance $l_1 = 0.42\,\mu$m corresponds to perfectly end-to-end aligned particles while $l_1 = 2\,\mu$m is a typical value found in experiments. The model based on the Eshelby/Mori Tanaka method is described in Ref. 22.

The effective composite properties are calculated using piezoelectric equivalents of Eshelby's tensors in combination with the Mori-Tanaka method.[36] This approach does not take into account the increased interaction between dielectrophoretically processed end-to-end aligned fibers. These models therefore underestimate the properties of DEP aligned composites. In Figure 20, an example is presented for a PZT volume fraction of $\varphi = 0.15$. The difference in behavior is most apparent for low aspect ratio particle inclusions. Here, the relative contribution of the end-to-end alignment is largest (see Eq. (17)). For large aspect ratio particles, the difference with the model from Eq. (26) disappears. The values for perfectly DEP aligned fibers (with inter particle spacing equal to the fiber surface roughness) and dilute dispersions represent the upper and lower bounds respectively.

CONCLUSIONS

Structured PZT short fiber–polymer composites were manufactured using dielectrophoresis. The orientation of the fibers progressively increases towards alignment in the direction of the electric field. The average length of the chains also increases due to the dielectrophoresis force.

Aspect ratio is of little influence on final structuring factor (in 2D). Possible cause is that the torque acting on the particles increases dramatically with aspect ratio. The final structuring factor decreases with volume fraction. This effect is more significant for 3D.

The microstructure of the composites in particular the average orientation of the fibers and aspect ratio of the fibers and the inter particle distance can be related to the piezoelectric properties of the composites. A model was developed which takes into account these properties. It successfully combines the effect of the particle aspect ratio and the inter particle distance on the electric field acting on the particle. Model predictions correlate well with experimental values for d_{33} and ε_{33} in the case of relatively low aspect ratio fibers. At higher aspect ratio fibers, the model slightly underestimates the properties of the composites. The g_{33} values for low volume fraction composites were found to increase with aspect ratio and orientation angle, with values rising to almost 15 times the value for bulk PZT.

ACKNOWLEDGMENTS

This work was financially supported by the SmartMix Programme of the Netherlands Ministry of Economic Affairs and the Netherlands Ministry of Education, Culture and Science (Grant SMVA0607). The authors are grateful to Morgan Electro Ceramics (Ruabon, United Kingdom) for providing the PZT powder and to the SMG group of Eindhoven University of Technology, for the use of their Berlincourt d_{33} meter. They would also like to thank Steve Perini for help with the alignment analysis setup. D. A. van den Ende acknowledges the tremendous hospitality at the Centre for Dielectric Studies (CDS) at The Pennsylvania State University where part of the research was conducted.

APPENDIX: EFFECTIVE INTER PARTICLE DISTANCE CALCULATION

In Figure 21, the relation of the values for $\tilde{\theta}$ and $\tilde{\theta}'$ is presented with the relation between the measured values and calculated values using the equivalent folded half normal distribution. The measured values for average orientation angle $\tilde{\theta}$ and standard deviation of the measurement $\tilde{\theta}'$ are compared to the angle at which the cumulative probability of the fitted distribution reaches 0.5 and the corresponding standard deviation of the fitted half normal distribution.

To calculate the effective value for C in Eq. (21), the effective inter particle distance, l_1, was calculated using the probability distribution of θ. The effective l_1 is equal to

$$l_{1,eff} = \frac{1}{\int_0^{\frac{\pi}{2}} \frac{p(\theta)}{R_a + \sin(\theta)\frac{w_2}{2}} d\theta}, \tag{A1}$$

where $p(\theta)$ is the probability distribution for θ. Using the relation between θ and θ', the average of l_1 can be plotted for θ'. In Figure 22, the result from Eq. (A1) is plotted and Eq. (21) is fitted to the data with least squares method, yielding a value of $C = 0.404$.

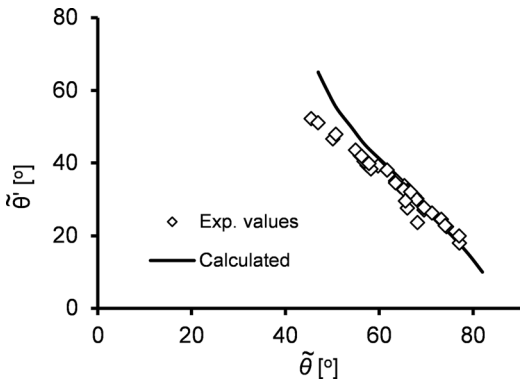

FIG. 21. The relation $\tilde{\theta}$ and $\tilde{\theta}'$ for all composite samples ($\tilde{\theta} = 90°$ yields $\tilde{\theta}' = 0°$ which means all particles are oriented perfectly in the direction of the electric field).

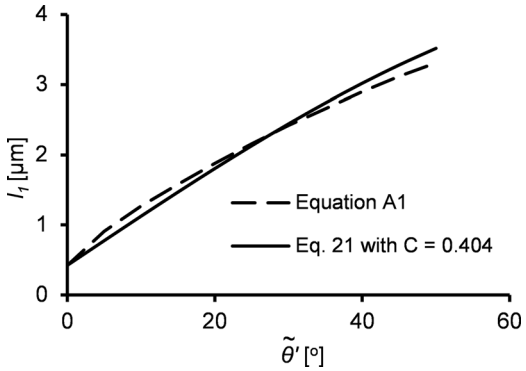

FIG. 22. Calculated values for l_1 using the probability distribution method compared to Eq. (21) ($C = 0.404$).

[1]R. E. Newnham, D. P. Skinner, and L. E. Cross, Mater. Res. Bull. **13**, 525 (1978).
[2]C. A. Randall, S. Miyazaki, K. L. More, A. S. Bhalla, and R. E. Newnham, Mater. Lett. **15**, 26 (1992).
[3]C. P. Bowen, A. S. Bhalla, R. E. Newnham, and C. A. Randall, J. Mater. Res. **9**, 781 (1994).
[4]M. Hase, M. Egashira, and N. Shinya, J. Intell. Mater. Syst. Struct. **10**, 508 (1999).
[5]V. Tomer, C. A. Randall, G. Polizos, J. Kostelnick, and E. Manias, J. Appl. Phys. **103**, 034115 (2008).
[6]D. A. van den Ende, H. J. van de Wiel, W. A. Groen, and S. van der Zwaag, Smart Mater. Struct. **21**, 01501 (2012).
[7]D. A. van den Ende, B. F. Bory, W. A. Groen, and S. van der Zwaag, J. Appl. Phys. **107**, 024107 (2010).
[8]C. P. Bowen, R. E. Newnham, and C. A. Randall, J. Mater. Res. **13**, 205 (1998).
[9]S. Yamashita, H. Hatta, T. Sugano, and K. Murayama, J. Compos. Mater. **23**, 32 (1989).
[10]J. Venermo and A. Sihvola, J. Electrost. **63**, 101 (2005).
[11]C. J. F. Böttcher, O. C. van Belle, P. Bordewijk, and A. Rip, *Theory of Electric Polarization* (Elsevier Scientific, 1978).
[12]A. Sihvola, *Electromagnetic Mixing Rules and Applications* (The Institution of Electrical Engineers, London, UK, 1999).
[13]T. B. Jones, *Electromechanics of Particles* (Cambridge University Press, Cambridge, UK, 1995), p. 119.
[14]T. B. Jones, IEEE Eng. Med. Biol. Mag. **22**, 33 (2003).
[15]W. T. Winter and M. E. Welland, J. Phys. D: Appl. Phys. **42**, 045501 (2009).
[16]G. B. Jeffery, Proc. R. Soc. London, Ser. A **102**, 161 (1922).
[17]J. M. Burgers, *Second Report on Viscosity and Plasticity* (North-Holland, Amsterdam, 1938).
[18]P. Dhar, T. M. Fischer, Y. Wang, T. E. Mallouk, W. F. Paxton, and A. Sen, Nano Lett. **6**, 66 (2006).
[19]M. L. Dunn and M. Taya, Proc. R. Soc. London, Ser. A **443**, 265 (1993).
[20]G. M. Odegard, Acta Mater. **52**, 5315 (2003).
[21]J. H. Huang and W. S. Kuo, Acta Mater. **44**, 4889 (1996).
[22]C. Andrews, Y. Lin, and H. A. Sodano, Smart Mater. Struct. **19**, 025018 (2010).
[23]H. L. W. Chan and J. Unsworth, IEEE Trans. Ultrason. Ferroelectr. Freq. Control **36**, 434 (1989).
[24]S. A. Wilson, G. M. Maistros, and R. W. Whatmore, J. Phys. D: Appl. Phys. **38**, 175 (2005).
[25]W. M. Chirdon, W. J. O'Brien, and R. E. Robertson, Dental Mater. **22**, 57 (2006).
[26]C. Sun, L. Qin, H. Xue, Z. Xiong, and Q. M. Wang, J. Appl. Phys. **107**, 024102 (2010).
[27]X. Y. Zhang, X. Zhao, C. W. Lai, J. Wang, X. G. Tang, and J. Y. Dai, Appl. Phys. Lett. **91**, 4190 (2004).
[28]N. Guo, S. A. Dibenedetto, P. Tewari, M. T. Lanagan, M. Ratner, and T. J. Marks, Chem. Mater. **22**, 1567 (2010).
[29]W. Cao, Q. M. Zhang, and L. E. Cross, J. Appl. Phys. **72**, 5814 (1992).
[30]Q. M. Zhang, W. Cao, H. Wang, and L. E. Cross, J. Appl. Phys. **73**, 1403 (1993).
[31]J. Feenstra and H. A. Sodano, J. Appl. Phys. **103**, 124108 (2008).
[32]C. Andrews, Y. Lin, H. Tang, and H. A. Sodano, J. Intell. Mater. Syst. Struct. **22**, 1879 (2011).
[33]H. Tang, Y. Lin, C. Andrews, and H. A. Sodano, Nanotechnology **22**, 015702 (2011).
[34]H. Tang, Y. Lin, and H. A. Sodano, Adv. Energy Mater. **2**, 469 (2012).
[35]H. Tang, Y. Lin, and H. A. Sodano, Proc. SPIE **7978**, 79780S (2011).
[36]T. Mori and K. Tanaka, Acta Metall. **21**, 571 (1973).